An Original Empirical Method for Simulating V L 2,3 Edges: The Example of KVPO4F and KVOPO4 Cathode Materials

Alessandro Longo, Romain Wernert, Antonella Iadecola, Christoph Sahle, Lorenzo Stievano, Laurence Croguennec, Dany Carlier, Alessandro Mirone

▶ **To cite this version:**

Alessandro Longo, Romain Wernert, Antonella Iadecola, Christoph Sahle, Lorenzo Stievano, et al.. An Original Empirical Method for Simulating V L 2,3 Edges: The Example of KVPO4F and KVOPO4 Cathode Materials. Journal of Physical Chemistry C, 2022, 126 (46), pp.19782-19791. ⟨10.1021/acs.jpcc.2c05334⟩. ⟨hal-03872596⟩

HAL Id: hal-03872596

https://cnrs.hal.science/hal-03872596v1

Submitted on 28 Nov 2022

HAL is a multi-disciplinary open access archive for the deposit and dissemination of scientific research documents, whether they are published or not. The documents may come from teaching and research institutions in France or abroad, or from public or private research centers.

L'archive ouverte pluridisciplinaire **HAL**, est destinée au dépôt et à la diffusion de documents scientifiques de niveau recherche, publiés ou non, émanant des établissements d'enseignement et de recherche français ou étrangers, des laboratoires publics ou privés.

HAL Authorization

An original empirical method for simulating V $L_{2,3}$ edges: the example of $KVPO_4F$ and $KVOPO_4$ cathode materials

Alessandro Longo,[*,†,‡,#] Romain Wernert,[¶,§,#] Antonella Iadecola,[§] Christoph J. Sahle,[†] Lorenzo Stievano,[‖,§,⊥] Laurence Croguennec,[¶,§,⊥] Dany Carlier,[¶,§,⊥] and Alessandro Mirone[*,†]

†*European Synchrotron Radiation Facility, 71, Avenue des Martyrs, Grenoble F-38000, France*

‡*Istituto per lo Studio dei Materiali Nanostrutturati (ISMN)-CNR, UOS Palermo, via Ugo La Malfa 153, Palermo 90146, Italy*

¶*Univ. Bordeaux, CNRS, Bordeaux INP, ICMCB, UMR 5026, F-33600 Pessac, France*

§*RS2E, Réseau sur le Stockage Electrochimique de l'Energie, FR CNRS 3459, Amiens F-80039, France*

‖*ICGM, Univ. Montpellier, CNRS, ENSCM, F-34100 Montpellier, France*

⊥*ALISTORE-ERI European Research Institute, FR CNRS 3104, F-80039 Cedex 1 Amiens, France*

#*R. Wernert and A. Longo contributed equally to this work.*

E-mail: alessandro.longo@esrf.fr; alessandro.mirone@esrf.fr

Phone: +33 (0)4 38881907;

Abstract

Reversible chemical reactions are the most common mechanism storing electrochemical energy in M-ion batteries (M = Li, Na, K...). At the positive electrode, these transformations consist in the solid-state oxidation or reduction of transition metal ions going along with the reversible (de)intercalation of an alkali cation from the crystal structure. X-ray spectroscopies are among the most suitable tools to unveil and monitor these reactions. The interpretation of experimental spectra, however, is not trivial. This is particularly true in V-based positive electrodes since the variety of oxidation states of vanadium as well as its coordination and bonding geometries may lead to complex spectroscopic features that call for *ab initio* modelling to understand the spectra. Here we show that V $L_{2,3}$-edge X-ray Raman spectra can effectively not only be modelled by a full *ab initio* approach, but also that the empirically obtained Hamiltonian parameters can reproduce shape and intensity of the experimental spectra from a given coordination geometry. In a broader context, our study shows that inexpensive empirical calculations provide highly reliable information and help solving the electronic structure of transition metal oxides compounds, which governs the electrochemical behaviour in M-ion battery. The promising results shown here underline the efficiency of this strategy for X-ray spectroscopy data analysis, that can be generalised and extended to the wider family of vanadium phosphate-based polyanionic compounds. Such an approach can in principle be extended to any transition metal based material.

Introduction

Vanadium is a versatile transition metal element, exhibiting a large variety of oxidation states ranging from +2 to +5 and very different coordination polyhedra including regular octahedra, strongly distorted octahedra, square based pyramids, as well as tetrahedra.[1,2] Such properties provide a rich crystal chemistry for V based compounds, especially phosphates. For this reason, many studies have been conducted in the field of battery electrode

materials based on V, such as LiV_2O_5,[3] $LiVPO_4F$,[4,5] $Na_3V_2(PO_4)_3$, $Na_3V_2(PO_4)_2F_3$[6–8] and many more. Indeed, electrochemical properties such as the potential window, the shape of the electrochemical curve or the capacity can be tailored by crystal structure and composition engineering.[8] For example, the preparation of mixed anion phosphates containing O and/or F allows triggering the $V^{5+/4+}$ or $V^{4+/3+}$ redox couples. Such materials were investigated for Li-ion batteries, Na-ion batteries and even K-ion batteries using, among others, $LiVPO_4F_{1-y}O_y$, $Na_3V_2(PO_4)_2F_{3-2y}O_{2y}$ and $KVPO_4F_{1-y}O_y$ ($0 \leq y \leq 1$).[9–12] In these compounds, for the case of oxygen-rich compositions containing only V^{4+}, a very short bond of 1.65 Å is formed between V and one of its surrounding oxygen atoms. Such a short bond distance is analogous to the vanadyl VO^{2+} ion and is referred to as a "vanadyl bond" depicted as V=O. Vanadyl bonding is a typical oxo-metal bond where the geometrical distortion lifts the t_{2g} degeneracy so that the d_{xy} orbital is solely occupied by the unpaired d^1 electron.[13] It also features strong π-bonding interactions between V d_{xz}, d_{yz} and the filled O $2p_x$, $2p_y$. Interestingly, some vanadium compounds exhibit multi-electron transfer properties such as tavorite $LiVOPO_4$, where Li^+ can be either deintercalated or intercalated from $LiVOPO_4$ to yield $VOPO_4$ or Li_2VOPO_4, by triggering the $V^{5+/4+}$ or $V^{4+/3+}$ redox couples respectively.[14,15] It was reported that VO_6 octahedra are distorted with a V=O bonding scheme in tavorite-type $VOPO_4$ and $LiVOPO_4$, whereas V lies in a symmetric octahedral coordination site in Li_2VOPO_4.[14] In addition, some unusual redox mechanisms were uncovered in $Na_3V_2(PO_4)_2F_3$. Upon charging, it was shown that the final composition $Na_1V_2(PO_4)_2F_3$ contained equal amounts of V^{5+} and V^{3+}, whereas only V^{4+} was expected.[16–18] Recent studies have also shown the formation of a short V-O bond upon charge of $Na_4FeV(PO_4)_3$.[19] Overall, vanadium battery materials show a wide variety of possible redox mechanisms and local environments, which are difficult to disentangle.

X-ray spectroscopy is the technique of choice especially at the V $L_{2,3}$ edges, which correspond to electronic transitions from occupied V $2p_{1/2}$ and $2p_{3/2}$ core levels to unoccupied

V $3d$ states ($2p^6\ 3d^n \rightarrow 2p^5\ 3d^{n+1}$). Such spectra are expected to carry information on oxidation state, local geometry and bonding. Probing these edges could help confirming both redox and structural mechanisms, as well as understanding unusual charge compensation processes. In spite of these promising features, the investigation of early $3d$ transition metal L-edges is sometimes hindered by both the spectral distortion and the surface sensitivity of total electron yield ($\approx$ 10 nm) and total fluorescence yield ($\approx$ 50 nm) soft X-ray absorption spectroscopy (soft-XAS) techniques.[20,21] X-ray Raman scattering (XRS) spectroscopy can overcome such issues since it relies on highly penetrating hard X-rays and an inelastic excitation process, thus providing bulk sensitivity. When the energy loss is close to the V $L_{2,3}$ edges excitation energies, the resulting XRS spectra contain information similar to the conventional soft-XAS ones. However, there are currently only few studies addressing properly the interpretation of V $L_{2,3}$ edge spectra by a calculation approach, limiting the thorough understanding of the carried information, especially about the electrochemical properties.[22–24] In the literature, two approaches tackling these problems are available. First, a rigorous *ab initio* quantum chemistry configuration interaction formalism is applied,[25–27] for a given crystallographic structure, and, importantly is parameterless. Such method has the advantage that molecular orbitals are optimised for each calculated excited state. However, these calculations are very demanding in terms of computing time, and this makes the comparison with experimental data a cumbersome procedure. In the second approach, a more straightforward formalism is implemented,[28–38] where a small cluster is considered but the orbitals are not optimised for the excited states. Instead a model Hamiltonian, with fixed empirical parameters, and modelled as a sparse matrix, acts on the second-quantisation vectorial space spanned by the cluster states. Then the spectra are efficiently calculated in the Krylov sub-space generated by recursive linear-algebra applications of the Hamiltonian. The inconvenience of the latter approach lies in the relatively high number of parameters to be tuned to calculate the crystal field. Moreover, two extra parameters are needed if hybridisation has to be considered. The total number of parameters, by neglecting the hybridisation, can

be reduced for high symmetry sites. Nevertheless, this is also multiplied by the number of non-equivalent sites. Since a direct link between the crystallographic structure and the used parameters is missing, data interpretation is not trivial. Even though some *ab initio* methods have been already proposed to control the free parameters, significant discrepancies between the calculated and the best fit crystal field parameters are still observed, which weaken the overall results.[39,40] In the methodology reported here, all the weaknesses are overcome by the novel approach implemented in Hilbert++ and reported below. Two different possible approaches within the code are here explored. The first case shows an improved Wannier approach, applied in a relaxed crystal structure, which overcomes the use of crystal field and hybridization parameters. In the second case, a semi-empirical method is adopted which involves the use of free parameters directly linked to the physics used to describe the system, such as hybridisation energy, crystal field and spatial position of the ligands around the transition metal. To highlight the elements of novelty a summary of the salient aspects of Hilbert++ code is reported in the next section. We apply our approach to experimental V $L_{2,3}$- and O K-edges XRS data of $KVPO_4F$ and $KVOPO_4$ cathode materials, which were used as references for V^{3+} and V^{4+}=O containing compounds. Accordingly, multiplet calculations of the V $L_{2,3}$ edges were conducted using the Hilbert++ code with the above introduced different approaches: i) the conventional one using the *ab initio* Hamiltonian obtained with localised Wannier orbitals from a full density functional theory (DFT) simulation; ii) an original and user-friendly method based on empirical parameters. In order to prove the complementarity of the two methodologies, a multi techniques approach is applied. More precisely, *ab initio* relaxed crystal structures resulting from GGA+U calculations with VASP were used to validate the experimental X-ray diffraction (XRD) crystal structures. Moreover, the relaxed structures were used as input for a DFT calculation, post-processed then with the Wannier90 code which sets the crystal field and hybridisation part of the Hamiltonian implemented in Hilbert++. The results are finally corroborated by spectral calculations at the O K-edge (see SI).

Remarkably, the combination of all such different theoretical approaches provides a complete picture of the electronic structure of the V atoms, which is directly linked to the distorted coordination geometry and electronic structure of the vanadium cations. Such distortion is hardly detected by Extended X-ray Absorption Fine Structure (EXAFS) analysis as the information contained in the spectra is averaged between the different oxygens and the features are less distinct.[12] The approach implemented in Hilbert++, instead, provides a full treatment of the correlation effects. These effects induce spectral features which are sufficiently resolved to be studied with our approach and, importantly, have different orbital characters with a rich dependence on the ligand environment, in particular for their relative variations.. Hilbert++ can also be applied using empirical parameters with a direct physical meaning such as ligand coordinates and Slater-Koster tight-binding parameters, thus allowing the qualitative recovery of structural information directly from the data without depending on expensive *ab initio* calculations. In conclusion, we show how such an empirical approach is a reliable and easy-to-use tool to correctly interpret XRS and XAS data.

Methods and experiments

Sample preparation

VPO_4 and $VOPO_4$ precursors were synthesized from $NH_4H_2PO_4$ (98 % Sigma-Aldrich) and V_2O_5 (99.6 %, Sigma-Aldrich). The powder mixture was heated to 800 °C for 10 hours under Ar/H_2 atmosphere to obtain VPO_4, which was oxidized in air at 750 °C for 5 hours to form $VOPO_4$. $KVPO_4F$ was then synthetized by mixing KF (Alfa Aesar) with VPO_4 in stoichiometric ratio. A pellet was placed in a sealed gold tube under argon (< 0.1 ppm H_2O/O_2) and calcination was performed at 650 °C for 6 hours. For $KVOPO_4$, the precursor mixture consisted in K_2CO_3 (Sigma-Aldrich, 99%), VPO_4 and $VOPO_4$ in a molar ratio. The pellet was calcined at 750°C under argon atmosphere. The samples studied are the same as those used in an earlier work where the precise control of anionic composition was

demonstrated.[12]

X-ray Raman Scattering (XRS) Spectroscopy measurement

XRS data were collected at beamline ID20 of the ESRF (Grenoble, France).[41] The pink beam from three U26 undulators was monochromatized at an incident energy of 9.6837 keV, using a cryogenically cooled Si(111) monochromator and a subsequent Si(311) channel-cut post-monochromator. The final beam was focused to a spot size of approximately 30 μm $\times$ 30 μm (V $\times$ H) at the sample position using a mirror system in Kirkpatrick-Baez geometry.

XRS is an inelastic X-ray scattering process, in which a high energy X-ray photon excites a core electron into an unoccupied state. At low transferred momenta, the process is, in principle, analogous to X-ray absorption spectroscopy (XAS), but the energy transfer to the outgoing photon plays the role of the X-ray photon energy absorbed in XAS. At high transferred momenta instead, compared to XAS, the spectra is enriched by the higher multipole contributions coming from the expansion of Eq. 4 in powers of Q. The large solid angle spectrometer at ID20 was used to collect XRS data with 36 spherically bent Si(660) crystal analysers. The data were extracted with the XRStools program package as described in detail elsewhere.[42] The sample was placed into the beam at 10° grazing incidence. All XRS measurements were carried out at room temperature. Full range scans were measured from 505 to 565 eV energy loss with a 1 eV step size. After acquisition of the survey scan, several detailed scans of specific edges were collected with a 0.2 eV step by scanning the incident beam energy to record energy losses in the vicinity of the V $L_{2,3}$-edge and O K-edge (505-565 eV). Acquisition scans lasted approximately 6 hours per sample. In order to be sure to hit always a fresh part of sample and to avoid radiation damage, the X-ray beam was moved on the sample during the measurement. Each XRS spectrum was recorded for about 10 minutes at a different spot of the sample, and no structural modification of the sample was observed during this time. All scans were checked for consistency before averaging over them. The overall energy resolution of the XRS spectra was 0.7 eV as estimated from the FWHM of

elastic scattering from a piece of adhesive tape.

Calculation scheme

Ab initio structural relaxation

DFT relaxed crystal structures of $KVPO_4F$ and $KVOPO_4$ were computed using the projector-augmented wave (PAW) method with the Vienna *ab initio* simulation package (VASP) code.[43–48] The generalized gradient approximation (GGA) with Perdew-Burke-Ernzerhof (PBE) exchange-correlation functional was used for all calculations.[49] A Hubbard correction (U_{eff}= U-J = 5 eV) was applied to take into account the self-interaction error of the strongly correlated $3d$ electrons.[50] $U_{eff} = 5$ eV was already used in previous studies of these compounds and provided a good agreement with experimental structure, voltage curve, and electronic structure.[12,51] All calculations were spin-polarized with ferromagnetic ordering.[52] The plane-wave cutoff energy was set to 600 eV and a 4×4×4 k-mesh was used. The octahedral distortion was calculated according to Equation 1 where d is a given bond distance among the first coordination shell and $\bar{d}$ is the average bond distance:

$$dist = \frac{1}{6}\sum_{i=1}^{6}\frac{(d_i - \bar{d})^2}{\bar{d}^2} \quad (1)$$

Hilbert++ and Wannier localized orbital

Multiplet calculations of the dynamic structure factor were performed with the Hilbert++ code.[53] Compared to other existing multiplet codes,[54,55] Hilbert++ allows to simulate local environments (*i.e.* first coordination sphere) of arbitrary symmetry[53] using few empirical Slater-Koster parameters, here detailed, and can simulate the XRS spectra and their momentum transfer (q) dependence. Moreover, alternatively to using empirical parameters, the code can extract the crystal field and hybridization Hamiltonian directly from modern *ab initio* codes, like Quantum Espresso (QE)[56,57] or the Vienna ab initio simulation package (VASP), through the Wannier90 code.[58,59]

For a simple cluster composed of a central ion and its surrounding coordinated , we calculate the photon scattering cross section due to the excitation of an initial cluster state $|i\rangle$, and an incoming photon at energy $\hbar\omega$ with polarisation ϵ, into one of the excited cluster states $|f\rangle$ and a scattered photon $\hbar\omega'$, as the dynamic structure factor obtained by this formula:

$$\frac{d^2\sigma}{d\Omega dE_{loss}} \propto \frac{\omega'}{\omega}(\epsilon'.\epsilon)\sum_n |\langle f\,|T_{b\leftarrow a}(\mathbf{Q})|\,i\rangle|^2\delta(E_f+\hbar(\omega'-\omega)-E_i) \tag{2}$$

where $T_{b\leftarrow a}$ expresses the action of the $\mathbf{A}^2$-term of the photon-electron Hamiltonian between two one-particle atomic spin-orbitals, with the annihilation $\hat{a}$ of an electron in (n_a, l_a, m_a, s) and the creation $\hat{b}^\dagger$ in (n_b, l_b, m_b, s):

$$T_{b\leftarrow a} = \sum_{m_b,m_a,s} t_{m_b,m_a}\hat{b}^\dagger_{m_b,s}\hat{a}_{m_a,s} \tag{3}$$

where the t coefficients are calculated, writing the atomic spin-orbitals as the product of a radial part,$\varphi_{n,l}(r)$, and angular part $Y^l_m(\mathbf{r}/r)$,[60] as :

$$t_{m_b,m_a} = \int \varphi_{n_b,l_b}(r)\varphi_{n_a,l_a}(r)/r^2 {Y^{l_b}_{m_b}}^\star(\mathbf{r}/r)Y^{l_a}_{m_a}(\mathbf{r}/r)exp(-i\mathbf{Q}.\mathbf{r})d\mathbf{r}^3 \tag{4}$$

The cluster wave-functions $|f\rangle$ and $|i\rangle$ are many-electrons eigen-functions of our cluster, the Hamiltonian can be written as:

$$H = H_{atomic} + H_{dd} + H_{dv} + H_{vv}. \tag{5}$$

The four contributing terms are, from left to right: the atomic Hamiltonian H_{atomic} of the central atom, the crystal field acting on the d electrons of vanadium H_{dd}, the hopping between the d orbitals and the $2p$ orbitals at the sites around the central vanadium atom H_{dv} (latter orbitals are represented by $\hat{v}^\dagger$, $\hat{v}$), and finally H_{vv}, the Hamiltonian governing the electron propagation over the neighbouring orbitals. The three latter contributions describe

the crystal field and the hybridisation:

$$H_{dd} + H_{dv} + H_{vv} = \sum_{m'ms} c_{m'm} \hat{d}^{\dagger}_{m',s} \hat{d}_{m,s} + \sum_{ims} \left(t_{i,m} \hat{v}^{\dagger}_{i,s} \hat{d}_{m,s} + c.c. \right) + \sum_{i,j,s} (t'_{i,j} + \delta_{ij}\Delta) \hat{v}^{\dagger}_{i,s} \hat{v}_{j,s}, \quad (6)$$

where the $3d$ orbitals are indexed by m, m', while i, j index the $\hat{v}$ orbitals and s is the spin. The coefficients c, t and t' are determined, based on the atomic positions, by two alternative methods: using maximally localized Wannier orbitals as calculated by the Wannier90 code, or empirical parameters. In the first approach, a self consistent field (SCF) *ab initio* calculation, using QE, is first performed using a local density approximation (LDA) functional. Then the Wannier90 code is used to form the maximally localised $3d$ wavefunctions of the selected vanadium site and, at the neighbouring oxygen and fluorine sites, the ligand $2p$ orbitals, which are possibly hybridised with the vanadium $3d$ electrons. Non equivalent vanadium sites are calculated independently and their spectra are averaged. The orbital synthesis is performed using an energy window, which encompasses both bonding and anti-bonding molecular orbitals.

The Wannier90 code outputs the tight-binding Hamiltonian matrix containing a first estimation of the c, t, and t' coefficients. A further refinement is made on the c factors to avoid double counting of the electron-electron interaction, which is already accounted for in H_{atomic}. This is realised by rotating the density matrix, given by the DFT code, obtaining its representation in the Wannier basis, and using it to extract the mean field approximation of electron-electron Coulomb operators of H_{atomic}. The result is subtracted from the matrix of c coefficients. This is at variance with what is described in[39] where the LDA potential is altered by removing the non-muffin-tin terms. We have verified that the estimated crystal field without this correction shows a poor agreement with the experimental one. Recently, a local electronic study on CO_3O_4 has been reported on the $2p - 3d$ transition where a clear discrepancy was observed between the best-fit $10Dq$ value, for the Co^{3+} site,

and the value obtained by the Wannier method.[40] Our proposed procedure, tested on this structure, produces $10Dq = 1.2eV$ which is close to their best-fit $10Dq$ up to 5%, while by removing the correction terms we obtain $10Dq = 0.66eV$ which is very close to their Wannier approximated value.

Another refinement is done introducing Δ as a free parameter of the model in equation 6. This parameter tunes the energy difference between the vanadium $3d$ and ligand $2p$ orbitals and it compensates for our ignorance about the very complex mechanism of screening, which occurs in particular for the $3d$ shell.

The H_{atomic} Hamiltonian is composed, in Hilbert++, by writing in second quantisation the Coulomb operators with their coefficients given by products of Slater integrals and angular moment coupling factors. The Slater integrals are reduced, following the standard procedure for multiplet calculations in the literature,[55] by a factor between 0.7 and 0.9 for multipoles of order $L > 0$; the monopole terms corresponding to $L = 0$ and strongly screened by the surrounding charge, are taken equal to 5.0 eV, which is in line with the U adopted in the literature for LDA+U calculation of vanadium phosphates.[12,51]

Alternatively to the *ab initio* calculation needed for the Wannier Hamiltonian, the crystal field and hybridisation contributions can be determined from empirical parameters. In this case the $t'_{i,j}$ matrix is diagonal, and is given by a free parameter (Δ), which tunes the energy difference between the vanadium $3d$ orbitals and the $2p$ orbitals of the ligands. Further, H_{dv} and H_{dd} are determined by two parameters each, one for σ- and the other for π-symmetry orbitals and by summing the contributions for each bonding vector $\mathbf{r}_b$, and re-scaling for each bond the interaction strength according to a power of the ratio $\frac{<r>}{r_b}$, with the average bond length.

In particular, introducing a Cartesian reference system (x_b, y_b, z_b) for each bond, aligned with $\mathbf{r}_b$ along the z_b axis, allow us to rewrite the H_{dv} and H_{dd} as follows:

$$H_{dv} = \sum_{b,s} \left(\frac{< r >}{r_b} \right)^3 \left(t_\sigma \hat{v}^\dagger_{z_b,s} \hat{d}_{z_b^2,s} + t_\pi (\hat{v}^\dagger_{x_b,s} \hat{d}_{x_b z_b,s} + \hat{v}^\dagger_{y_b,s} \hat{d}_{y_b z_b,s}) \right) + c.c. \tag{7}$$

and

$$H_{dd} = \sum_{b,s} \left(\frac{< r >}{r_b} \right)^3 \left(c_\sigma \hat{d}^\dagger_{z_b^2,s} \hat{d}_{z_b^2,s} + c_\pi (\hat{d}^\dagger_{x_b z_b,s} \hat{d}_{x_b z_b,s} + \hat{d}^\dagger_{y_b z_b,s} \hat{d}_{y_b z_b,s}) \right). \quad (8)$$

Finite Difference Method Near-Edge Structure (FDMNES) approach

To validate the electronic structure of the materials, O K-edge *ab initio* simulations were performed using FDMNES software package.[61] This code is particularly suited for X-ray absorption near-edge structure (XANES) simulations within the one-particle potential approximation. Therefore it is not appropriated for multiplet calculations but can treat large systems where correlation weakly affect the spectra. The atomic positions were generated from the crystallographic data reported in a previous work.[12] Moreover, the simulations were also performed on the two different $KVOPO_4$ and $KVPO_4F$ structures previously relaxed by DFT calculation with VASP and using GGA+U with $U_{eff} = 5$ eV. The simulations of the O K-edge spectra were performed by using multiple scattering theory based on the muffin-tin (MT) approximation for the potential shape of the Green scheme, non-relativistic calculations and the Hedin–Lundqvist exchange.[61] The MT radii were tuned to have a proper overlap between the different spherical potentials. The approximation of non-excited scatterers was used. Finally, an arc-tangent convolution to account for the core-hole lifetime and photoelectron state width was performed, followed by a Gaussian convolution. This last step is necessary to consider the experimental resolution. The obtained spectra were then normalized to the same integrated intensity of the experimental data in the suitable energy loss range. To take into account the ionic character of the oxygen atom, the dilatorb parameter m, available in the FDMNES code, was considered. This parameter modifies the spatial extent of the valence orbitals, hence allowing one to alter the degree of covalency. Moreover, it also takes into account the actual charge of the oxygen species at the O K-edge. Dilatorb can be adopted for each ionic species in the material, depending on the investigated edge, but it was mainly applied on the O^{2-} anion, the atomic basis of which is generally taken from the neutral atom to simulate the O K-edge data.

Results and discussion

Homeotypic $KVOPO_4$ and $KVPO_4F$ crystallize in the $KTiOPO_4$ (KTP) type structure ($Pna2_1$).[62,63] For $KVPO_4F$, the framework can be described by infinite corner-sharing VO_4F_2 chains linked by F atoms. Phosphate groups hold the chains together and large channels can accommodate K^+ ions. Two symmetrically nonequivalent vanadium sites exist, with either a *cis* or *trans* arrangement of the F^- ligands. In $KVOPO_4$, fluorides are substituted by O^{2-}, which implies an oxidation state of +4 for the vanadium and consequently the $V^{4+}O_6$ octahedra are strongly distorted in order to stabilise the d^1 electron configuration. The experimental crystal structure and V-O/F bond lengths of each V site in $KVPO_4F$ and $KVOPO_4$ are presented in Figure 1.

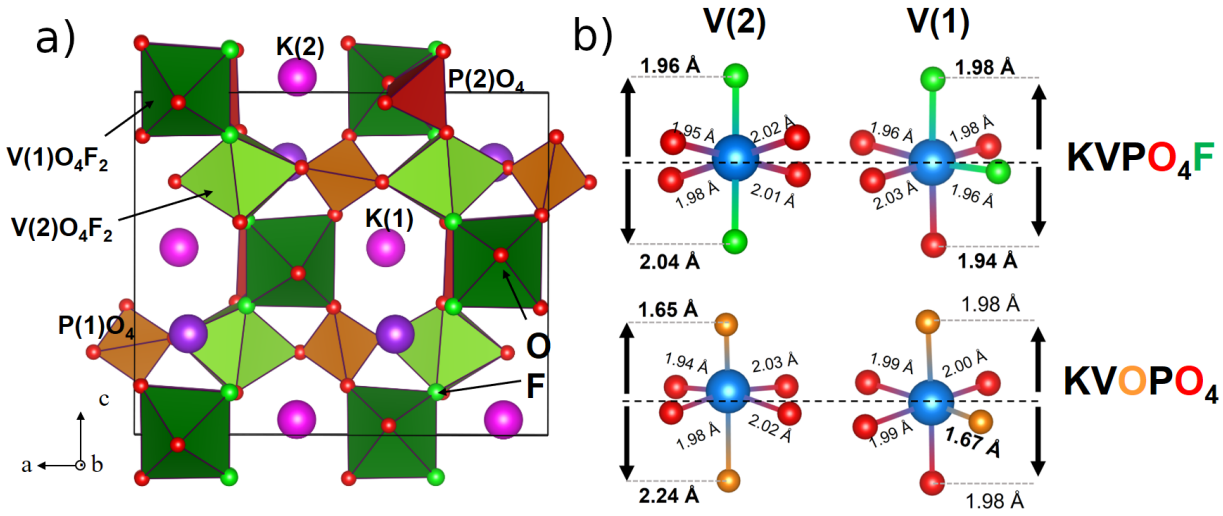

Figure 1: a) Crystal structure of $KVPO_4F$. The F sites can be completely or partially substituted by oxygen, up to the composition $KVOPO_4$. b) Detailed experimental bond length of the first coordination shell in $KVPO_4F$ (top) and $KVOPO_4$ (bottom) for both vanadium sites.

Figure 2 shows the experimental XRS spectra for the vanadium fluoride phosphate $KVPO_4F$ and vanadium oxide phosphate $KVOPO_4$. V$L_{2,3}$ edges correspond to excitations from the $2p^6\ 3d^n$ V ground state towards the $2p^5\ 3d^{n+1}$ V states. The two major features of these edges are the strong white-lines L_3 and L_2 due to the spin orbit splitting of the vana-

dium $2p$ core hole and separated by about 6.5 eV. Additional pre-peak features appearing at lower energies of the two main L_3, L_2 peaks, marked by arrows, can be observed. A chemical shift of 1.3 eV is measured, at the maximum of the V L_3 line, between the V^{4+} and the V^{3+} compound.

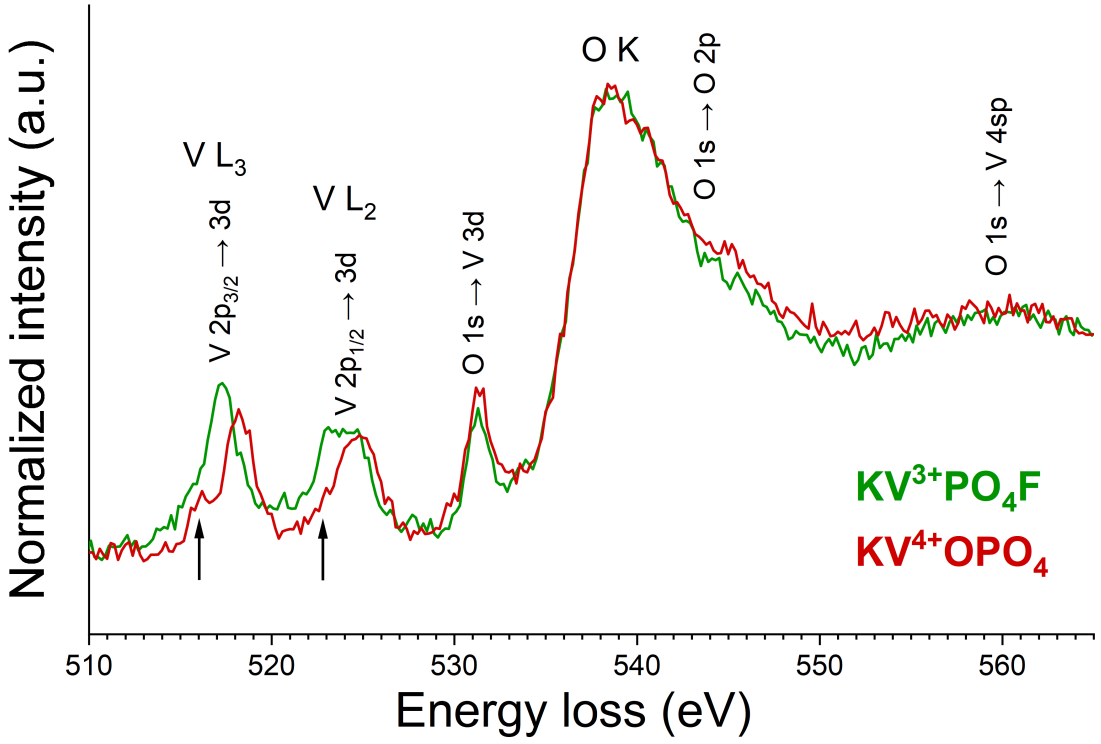

Figure 2: Experimental XRS spectra at the $L_{2,3}$ and O K edges of $KVPO_4F$ and $KVOPO_4$. The arrows point out the pre-peaks of the L_3 and L_2 white lines.

As witnessed by the change of the peak ratio at the $L_{2,3}$ edges shown in Figure 2, the increase of fluorine content in the structure induces a modification of the electronic state of vanadium. We observe a variation of the integrated L_3/L_2 ratio from 0.98 to 0.85 while the absolute intensity L_3/L_2 ratio changes from 1.38 to 1.25 between $KVPO_4F$ and $KVOPO_4$. The very slight variation of the oxygen K-edge features are localised in the pre-edge region between 530 and 535 eV. To directly correlate the electronic structure modifications with the changes occurring at the vanadium edge, multiplet calculations were performed using Hilbert++.

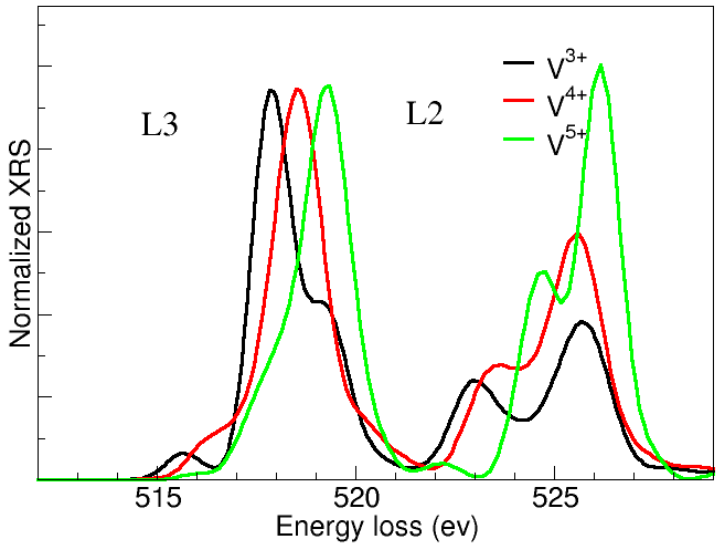

Figure 3: Simulation of different nominal vanadium ions, without any crystal field nor hybridisation, obtained with Hilbert++ code.

A preliminary simulation of the $L_{2,3}$ edges for different vanadium isolated ions V^{n+} (n=3,4,5) is reported in Figure 3. From these curves one can evaluate, in the absence of any ligand field and orbital hybridisation effect, the impact of solely varying the $3d$ occupancy from $n_{3d} = 0$ for V^{5+} to $n_{3d} = 2$ for V^{3+} on the spectra. In agreement with the literature, ([64] section VI.B) these simulations show that the L_3/L_2 peak ratio increases when the occupancy increases from V^{5+} to V^{3+}. This results is expected as the L_3/L_2 ratio depends on the interplay between the vanadium $2p$ spin-orbit coupling and the action of direct and exchange Coulomb interaction between vanadium $2p$ and $3d$ orbitals.

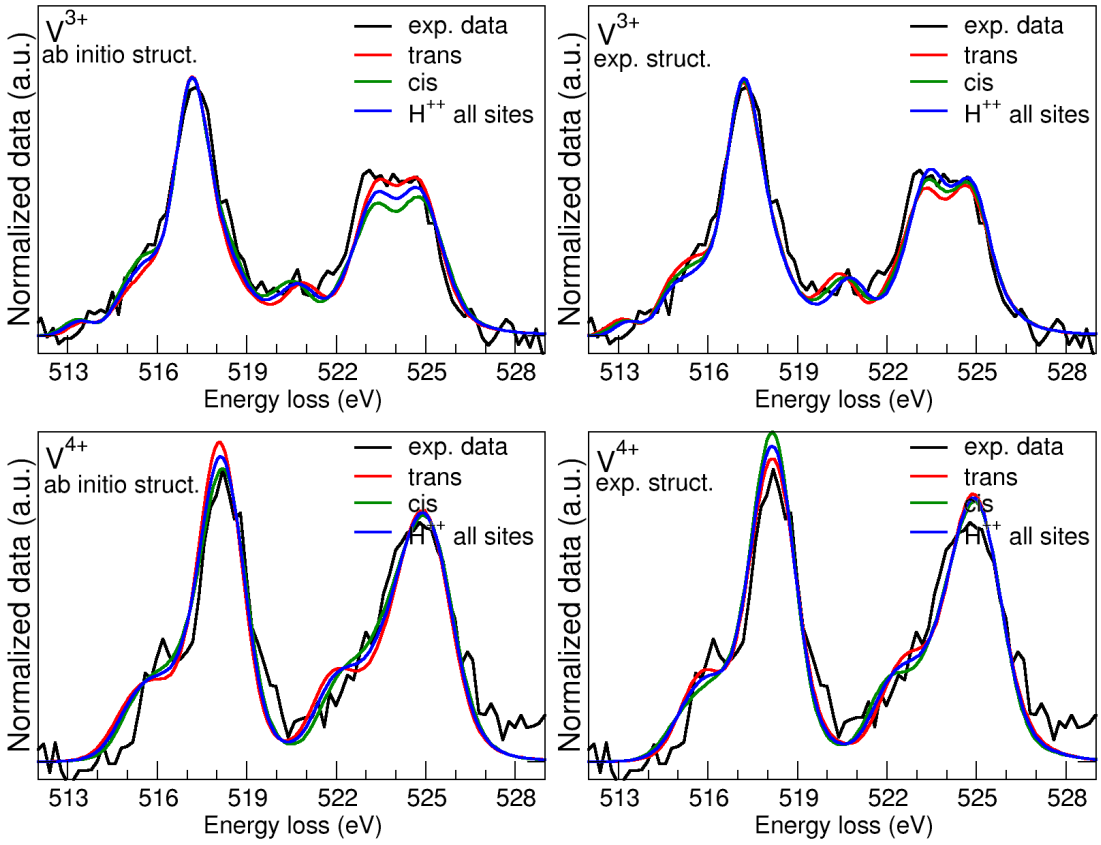

Figure 4: Energy loss spectra for $KVPO_4F$ and $KVOPO_4$ systems. The corresponding V^{3+} and V^{4+} spectra are calculated on the basis of the Wannier Hamiltonian for the *ab initio* structures (left panel) and experimental structures (right panel).

The multiplet simulations of $KVPO_4F$ and $KVOPO_4$ (containing V^{3+} and V^{4+}, respectively) are shown in Figure 4. These simulations are obtained on the basis of the Wannier Hamiltonian for the *ab initio* optimised structures (left panels) and for the experimental structure (right panels), with the V^{3+} system in the upper row and V^{4+} in the lower one. The Slater integrals reduction factor that were applied are 0.8 for V^{3+} and 0.7 for V^{4+}.

It should be pointed out that once the Slater integral reduction factor is fixed, only one free parameter Δ (see equation 6) is needed for the simulation employing the localized Wannier orbitals as input. We recall that Δ tunes the energy difference between $3d$- and neighbouring ligand $2p$-orbitals and thus the value of such free parameter has been fixed by considering that the oxidation process tends to re-equilibrate the electron affinity of the

different ionic species. Therefore, Δ is calculated such that the HOMO is evenly shared between the vanadium $3d$ and the ligand $2p$ orbitals when, to disentangle the Δ parameter from the value of the hopping terms, the hopping term is strongly reduced. This is simply obtained by scaling down the t factors to below 10^{-2} eV. When the code is used with a realistic hopping strength the HOMO-LUMO gap is increased and the HOMO character is clearly V-$3d$ like.

The resulting approximated crystal field $10\overline{Dq}$ parameter,[55] defined here as $10\overline{Dq}$, and the electron π-bonding charge δq are displayed in Table 1. The π-bonding charge, δq, is the difference between the average occupancy of the $3d$ shell in the ground state and the nominal occupancy. The parameter $10\overline{Dq}$, instead, is deduced from the H_{dd} term, which can always be written as a cubic (local) symmetry term plus a perturbation term with possibly no symmetry, *i.e.* the difference between the average energy of the perturbed e_g levels and the average of the perturbed t_{2g} levels (see Figure 1 S1 in SI). In practice, to monitor the strength of the H_{dd} term, the matrix is diagonalized and 5 levels are obtained. Then, the $10\overline{Dq}$ monitor is provided as the difference between the center of gravity, by considering separately the average energy of the upper two levels (perturbed e_g's) and of the the lower three ones (perturbed t_{2g}'s). As an additional monitor value, Δ_{CF}, defined as the maximum absolute distance between a crystal field split level and the center of gravity of its perturbed group (perturbed e_g's or t_{2g}'s) is also introduced. In O_h symmetry $10\overline{Dq}$ is equal to $10Dq$, with $\Delta_{CF} = 0$ (Figure S1 in SI), while it would be equal to $5/(3\sqrt{30})X_{400}$ in a regular T_d symmetry. A high value of Δ_{CF} indicates the necessary condition of strong departure from octahedral symmetry, which still is not a sufficient condition for detecting an high Δ_{CF}. In fact, the departure can be realised also in the eigenvector space.

Table 1: Local environment effect on the V ions in the calculations with Wannier Hamiltonian.

	vasp struct.			exp. struct.		
	$10\overline{Dq}$ (eV)	Δ_{CF} (eV)	δq	$10\overline{Dq}$ (eV)	Δ_{CF} (eV)	δq
V^{3+}_{cis}	1.33	0.13	0.39	1.44	0.1	0.39
V^{3+}_{trans}	1.24	0.27	0.40	1.37	0.24	0.40
V^{4+}_{cis}	1.37	0.47	0.43	1.25	0.39	0.44
V^{4+}_{trans}	1.34	0.39	0.43	1.07	0.1	0.44

The analysis of the values summarized in Table 1, shows that the crystal field monitor values $10\overline{Dq}$ and Δ_{CF} are compatible with a slight deviation of the crystal field from O_h symmetry, with an increased Δ_{CF} for the *trans* configuration, which aligns two fluorine ions on the same axis. We notice a discrepancy for $10\overline{Dq}$ between the V^{4+}_{trans} experimental and *ab initio* cases. This discrepancy is found also in the geometrical distortion: in the experimental structure, the very short vanadyl bond is mirrored on the opposite side by an elongated bond (see Figure 1). This elongation probably plays a compensation role for the stabilisation of the crystal structure, even though in the *ab initio* calculated structure it is less pronounced. Besides depending on the crystal field, the local environment also depends on the neighbouring orbitals and their hybridisation with the vanadium $3d$ ones. By inspection of the t' term of Eq. 6 it can be observed that the $2p$ orbitals of fluorine, in the V^{3+} system, have an average energy of about 1.5 eV lower than those of the oxygen ligands. Concerning V^{4+} instead, the oxygen-vanadium hopping t' terms are 57% stronger for the short vanadyl bond than for the other longer bonds, while the $2p$ average energy on the oxygen V-V bridge sites are 0.8 eV higher than that of the other oxygen sites. The agreement with the experiment is quite satisfactory, especially considering that all parameters are determined from the *ab initio* electronic structure. In particular, apart from a rigid shift in energy and an overall intensity rescaling, no fitting procedure was applied. The rigid shift is necessary because, at variance with the *ab initio* quantum chemistry configuration interaction codes,

the relaxation processes occurring in the final state atomic orbitals are not described in our model Hamiltonian. This results in over-estimated transition energies. The scaling is also needed as the experimental protocol does not contemplate the absolute calibration of the signal, which would require a laborious procedure to acquire a full characterisation of the beam shape, the exact density distribution of the sample, and the calculation of the scattering paths through the sample. The same rescaling factor is applied to the pairs of *trans* and *cis* sites.

Such results were obtained for an a *a priori* known stable structure, used here as a reference system. For measurements carried out in *operando* conditions, it may happen that the system is far from equilibrium and its configuration is difficult to catch by *ab initio* calculations, which may converge to a different stable structure.

In order to understand which structural information can be obtained from multiplet simulation, the calculation was repeated, matching the experimental data by using the empirical parameters instead of the Wannier Hamiltonian. Accordingly, the complementary nature of the two approaches can be proved.

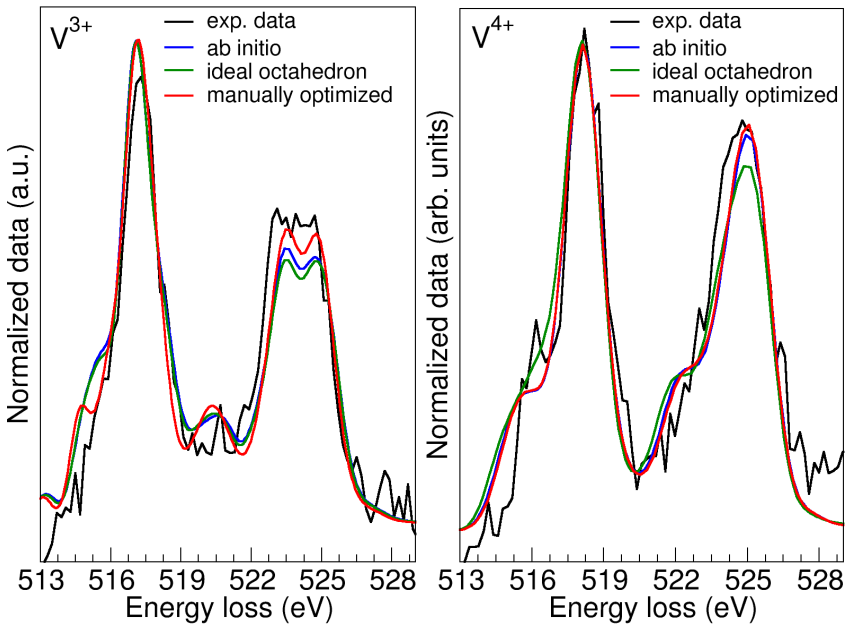

Figure 5: Simulation of V^{3+} and V^{4+} XRS spectra with Hilbert++ and optimal empirical parameters considering a distorted octahedron given by *ab initio* optimisation (blue line), an ideal octahedron (green line), and finally a distorted octahedron whose coordinates have been manually optimised (red line).

Figure 5 shows the simulations obtained by varying the empirical parameters, first by fixing the geometry and letting only the hybridisation and crystal field parameters to vary (green curve), then by manually distorting the octahedra (red curve). During the manual optimisation of the structure the hybridisation parameters are kept constant because they are transferable. The spectra obtained fixing the ionic positions to the DFT optimised structure are shown for comparison (blue curve). The empirical parameters are reported in Table 2.

Table 2: Empirical crystal field and hopping parameters used for V^{3+} and V^{4+}.

Empirical parameter	Value(eV)
c_σ	0.6
c_π	0.0
t_σ	1.0
t_π	0.5

The same set of crystal field and hybridisation parameters was used for the two systems, as they are transferable parameters, which are rescaled according to the geometry in Eq.

(7,8). Tables 3 and 4 display the ligand positions for the V sites in (0,0,0) position, which are drawn in Figure 6:

Table 3: Local structure of VO_6 octahedron in $KVOPO_4$. Distances are reported in Å.

	V^{4+} vasp			V^{4+} manually opt.		
Ligand	x	y	z	x	y	z
O_1	0	0	2.06	0	0	2.0
O_2	-0.23	0.005	-2.02	0	0.0	-2.0
O_3	1.73	0	-0.1	1.6	0	0
O_4	-2.05	-0.23	-0.17	2.0	0	0
O_5	-0.144	1.98	-0.14	0	2.0	0
O_6	-0.195	-1.98	-0.05	0	-2.0	-0

Table 4: Local structure of VO_4F_2 octahedron in $KVPO_4F$

	V^{3+} vasp			V^{3+} manually opt.		
Ligand	x	y	z	x	y	z
F_1	0	0	2.04	0	0	2.28
F_2	0.08	-0.1	-2.02	0	0	-2.28
O_1	2.02	0	0.07	2	0	0
O_2	-2.01	-0.1	0.2	-2	0	0
O_3	-0.01	2.02	-0.2	0	2	0
O_4	0.01	-2.06	0.2	0	-2	0

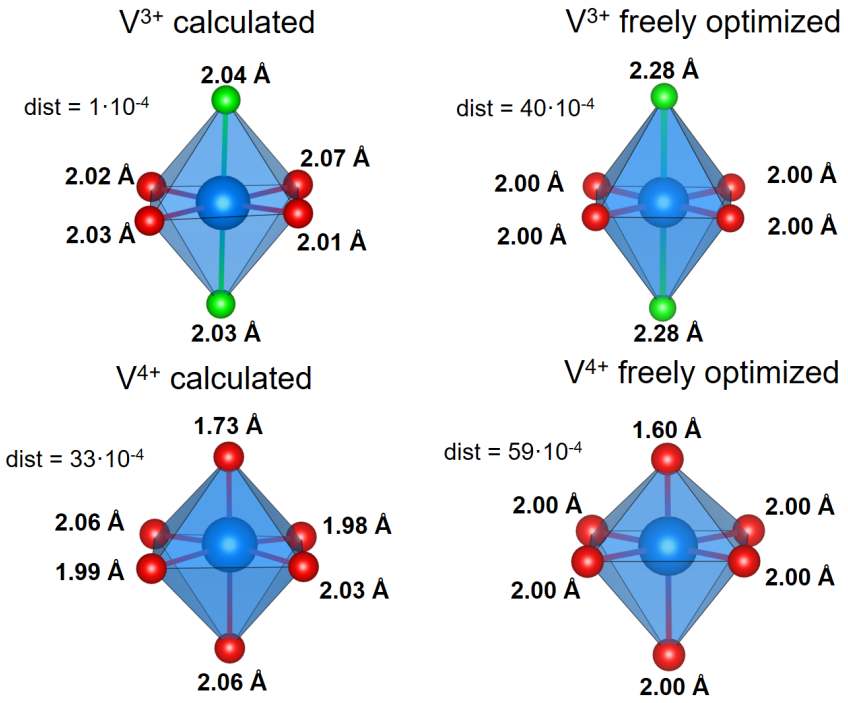

Figure 6: Local environments of V^{3+} and V^{4+} sites corresponding to Tables 3 and 4.

The resulting approximated crystal field $10\overline{Dq}$, and electron π-bonding charge δq are displayed in Table 5.

Table 5: Local environment indicators in the non distorted case.

	$10\overline{Dq}$ (eV)	Δ_{CF} (eV)	δq
V^{3+} vasp	1.8	0.03	0.38
V^{4+} vasp	1.81	0.15	0.42
V^{3+} manually set	1.85	0.22	0.39
V^{4+} manually set	1.9	0.26	0.43
V^{3+} octahedra	1.8	0.0	0.38
V^{4+} octahedra	1.8	0.0	0.42

Figure 5 shows that the simulations for the V^{3+} system are in good agreement for all three considered structures, of which the VASP optimized and manually optimised structure show slightly better agreement with experiment than the simulation based on an ideal octahedron. For this system, Figure 5 only shows the *trans* structure as it is clear based on the *ab initio* simulations that the differences between the spectra of the *cis* and *trans* forms are

negligible. Starting from the octahedron and manually setting the ionic positions along the *trans* axis(red curve), a slight improvement of the simulation of the ratio of the two edges could be obtained. Along this axis, in fact, the hybridisation of the fluorine atoms depends, in a real system, not only on the V-F distance but also on the fluorine energy, which is different than the oxygen one (see the above discussion on the Wannier90 derived Hamiltonian). As the actual version of Hilbert++ considers, in the empirical model, all ligand orbitals as degenerate, the extra distortion along the fluorine axis mimics, by using positional parameters, the effect of such degeneracy removal on the spectra. It can be noted that the best simulations of experimental spectra was achieved with longer V-F distances (2.28 Å) than V-O (2 Å). Even though different from what is experimentally observed, it can be explained by considering that F^- $2p$ orbitals are more contracted than O^{2-} such that, in an empirical simulation, this effect is accounted by longer V-F distances. This observation opens the door to future developments of the empirical model of the Hilbert++ code, where the parameters will be adapted to the nature of the different ligands.

For the V^{4+} system, we found that the distortion plays a significant role by improving the ratio of the L_3 and L_2 edges. The contraction describing the vanadyl bond in the manually-modified positions from the regular octahedron, is sufficient to improve the agreement with the experimental data, and a similar results is obtained with the structure derived from DFT relaxation.

Conclusion

In this work, experimental XRS spectra at the V $L_{2,3}$- and O K-edges of $KVPO_4F$ and $KVOPO_4$ are interpreted based on the results of full charge transfer multiplet simulations with different approaches to approximate the Hamiltonian of the site environment. In particular, it is shown how spectra simulated either using empirical parameters or by a full *ab initio* treatment of the problem confirm the presence of a distorted local environment of the V^{4+}

ions, whereas only subtle differences exist between the heteroanionic *cis* or *trans* arrangements. Simulations of the oxygen K-edge using a multiple scattering approach corroborates these results (see SI).

The perspective of using inexpensive empirical calculations arises as a very powerful tool for the analysis, the understanding, and the prediction of transition metal L-edges X-ray spectroscopy. Such calculations can be easily carried out on the fly by material science researchers, and can be of particular help when investigating the redox mechanisms at the atomic scale in transition metals compounds as electrode materials for M-ion batteries.

Acknowledgement

We acknowledge the European Synchrotron Radiation Facility for provision of synchrotron radiation facilities. The authors gratefully acknowledge financial support from the French National Research Agency (projects *Labex STORE-EX*, grant no. ANR-10-LABX-76–01 and *TROPIC*, grant no. ANR-19-CE05-0026). F. Gerbon is acknowledged for technical support before and during the experiment at ID20.

Supporting Information Available

Additional experimental results of O K edge are here fully described. This material is available free of charge via the Internet at http://pubs.acs.org.

References

(1) Boudin, S.; Guesdon, A.; Leclaire, A.; Borel, M.-M. Review on vanadium phosphates with mono and divalent metallic cations: syntheses, structural relationships and classification, properties. *International Journal of Inorganic Materials* **2000**, *2*, 561–579.

(2) Schindler, M.; Hawthorne, F. C.; Baur, W. H. Crystal chemical aspects of vanadium: polyhedral geometries, characteristic bond valences, and polymerization of (VO_n) Polyhedra. *Chemistry of Materials* **2000**, *12*, 1248–1259.

(3) Cocciantelli, J. M.; Ménétrier, M.; Delmas, C.; Doumerc, J. P.; Pouchard, M.; Hagenmuller, P. Electrochemical and structural characterization of lithium intercalation and deintercalation in the γ-LiV_20_5 bronze. *Solid state ionics* **1991**, 7.

(4) Barker, J.; Gover, R.; Burns, P.; Bryan, A.; Saidi, M.; Swoyer, J. Structural and electrochemical properties of lithium vanadium fluorophosphate, $LiVPO_4F$. *Journal of Power Sources* **2005**, *146*, 516–520.

(5) Gover, R.; Burns, P.; Bryan, A.; Saidi, M.; Swoyer, J.; Barker, J. $LiVPO_4F$: A new active material for safe lithium-ion batteries. *Solid State Ionics* **2006**, *177*, 2635–2638.

(6) Serras, P.; Palomares, V.; Goñi, A.; Gil de Muro, I.; Kubiak, P.; Lezama, L.; Rojo, T. High voltage cathode materials for Na-ion batteries of general formula $Na_3V_2O_{2x}(PO_4)_2F_{3\text{-}2x}$. *Journal of Materials Chemistry* **2012**, *22*, 22301.

(7) Serras, P.; Palomares, V.; Alonso, J.; Sharma, N.; López del Amo, J. M.; Kubiak, P.; Fdez-Gubieda, M. L.; Rojo, T. Electrochemical Na extraction/insertion of $Na_3V_2O_{2x}(PO_4)_2F_{3-2x}$. *Chemistry of Materials* **2013**, *25*, 4917–4925.

(8) Masquelier, C.; Croguennec, L. Polyanionic (phosphates, silicates, sulfates) frameworks as electrode materials for rechargeable Li (or Na) batteries. *Chemical Reviews* **2013**, *113*, 6552–6591.

(9) Nguyen, L. H.; Broux, T.; Camacho, P. S.; Denux, D.; Bourgeois, L.; Belin, S.; Iadecola, A.; Fauth, F.; Carlier, D.; Olchowka, J.; Masquelier, C.; Croguennec, L. Stability in water and electrochemical properties of the $Na_3V_2(PO_4)_2F_3$ – $Na_3(VO)_2(PO_4)_2F$ solid solution. *Energy Storage Materials* **2019**, *20*, 324–334.

(10) Broux, T.; Bamine, T.; Fauth, F.; Simonelli, L.; Olszewski, W.; Marini, C.; Ménétrier, M.; Carlier, D.; Masquelier, C.; Croguennec, L. Strong impact of the oxygen content in $Na_3V_2(PO_4)_2F_{3-y}O_y (0 \leq y \leq 0.5)$ on its structural and electrochemical properties. *Chemistry of Materials* **2016**, *28*, 7683–7692.

(11) Boivin, E.; David, R.; Chotard, J.-N.; Bamine, T.; Iadecola, A.; Bourgeois, L.; Suard, E.; Fauth, F.; Carlier, D.; Masquelier, C.; Croguennec, L. $LiVPO_4F_{1-y}O_y$ tavorite-type compositions: influence of the concentration of vanadyl-type defects on the structure and electrochemical performance. *Chemistry of Materials* **2018**, *30*, 5682–5693.

(12) Wernert, R.; Nguyen, L. H. B.; Petit, E.; Camacho, P. S.; Iadecola, A.; Longo, A.; Fauth, F.; Stievano, L.; Monconduit, L.; Carlier, D.; Croguennec, L. Controlling the cathodic potential of $KVPO_4F$ through oxygen substitution. *Chemistry of Materials* **2022**, 13.

(13) Ballhausen, C. J.; Gray, H. B. The electronic structure of the vanadyl ion. *Inorganic Chemistry* **1962**, *1*, 111–122.

(14) Bianchini, M.; Ateba-Mba, J. M.; Dagault, P.; Bogdan, E.; Carlier, D.; Suard, E.; Masquelier, C.; Croguennec, L. Multiple phases in the ϵ-VPO_4O - $LiVPO_4O$ - Li_2VPO_4O system: a combined solid state electrochemistry and diffraction structural study. *J. Mater. Chem. A* **2014**, *2*, 10182–10192.

(15) Wangoh, L. W. et al. Uniform second Li ion intercalation in solid state ϵ-$LiVOPO_4$. *Applied Physics Letters* **2016**, *109*, 053904.

(16) Bianchini, M.; Fauth, F.; Brisset, N.; Weill, F.; Suard, E.; Masquelier, C.; Croguennec, L. Comprehensive Investigation of the $Na_3V_2(PO_4)_2F_3$ - $NaV_2(PO_4)_2F_3$ System by Operando High Resolution Synchrotron X-ray Diffraction. *Chem. Mater.* **2015**, 12.

(17) Broux, T.; Bamine, T.; Simonelli, L.; Stievano, L.; Fauth, F.; Ménétrier, M.; Carlier, D.; Masquelier, C.; Croguennec, L. V^{IV} Disproportionation upon sodium extraction from $Na_3V_2(PO_4)_2F_3$ observed by operando x-ray absorption spectroscopy and solid-state NMR. *The Journal of Physical Chemistry C* **2017**, *121*, 4103–4111.

(18) Nguyen, L. H. B.; Iadecola, A.; Belin, S.; Olchowka, J.; Masquelier, C.; Carlier, D.; Croguennec, L. A combined operando synchrotron x-ray absorption spectroscopy and first-principles density functional theory study to unravel the vanadium redox paradox in the $Na_3V_2(PO_4)_2F_3$ – $Na_3V_2(PO_4)_2FO_2$ compositions. *The Journal of Physical Chemistry C* **2020**, *124*, 23511–23522.

(19) Park, S.; Chotard, J.-N.; Carlier, D.; Moog, I.; Duttine, M.; Fauth, F.; Iadecola, A.; Croguennec, L.; Masquelier, C. An asymmetric sodium extraction/insertion mechanism for the Fe/V-mixed NASICON Na_4 $FeV(PO_4)_3$. *Chemistry of Materials* **2022**, acs.chemmater.2c00501.

(20) Frati, F.; Hunault, M. O. J. Y.; de Groot, F. M. F. Oxygen K-edge x-ray absorption spectra. *Chemical Reviews* **2020**, *120*, 4056–4110.

(21) Fehse, M.; Iadecola, A.; Simonelli, L.; Longo, A.; Stievano, L. The rise of x-ray spectroscopies for unveiling the functional mechanisms in batteries. *Phys. Chem. Chem. Phys.* **2021**, *23*, 23445–23465.

(22) Hébert, C.; Willinger, M.; Su, D.; Pongratz, P.; Schattschneider, P.; Schlögl, R. Oxygen K-edge in vanadium oxides: simulations and experiments. *The European Physical Journal B* **2002**, *28*, 407–414.

(23) Willinger, M. G.; Su, D. S.; Schlögl, R. Electronic structure of β-$VOPO_4$. *Physical Review B* **2005**, *71*, 155118.

(24) Firet, N. J.; Venugopal, A.; Blommaert, M. A.; Cavallari, C.; Sahle, C. J.; Longo, A.; Smith, W. A. Chemisorption of anionic species from the electrolyte alters the surface

electronic structure and composition of photocharged $BiVO_4$. *Chemistry of Materials* **2019**, *31*, 7453–7462.

(25) Brik, M. G.; Ogasawara, K.; Ikeno, H.; Tanaka, I. Fully relativistic calculations of the L-2,L-3-edge XANES spectra for vanadium oxides. *European Physical Journal B* **2006**, *51*, 345–355.

(26) Hoeche, T.; Ikeno, H.; Maeder, M.; Henderson, G. S.; Blyth, R. I. R.; Sales, B. C.; Tanaka, I. Vanadium L-2,L-3 XANES experiments and first-principles multielectron calculations: impact of second-nearest neighboring cations on vanadium-bearing fresnoites. *American Mineralogist* **2013**, *98*, 665–670.

(27) Aquilante, F. et al. Modern quantum chemistry with [Open]Molcas. *The Journal of Chemical Physics* **2020**, *152*, 214117.

(28) Abbate, M.; Pen, H.; Czyzyk, M.; De Groot, F.; Fuggle, J.; MA, Y.; Chen, C.; Sette, F.; Fujmori, A.; Ueda, Y.; Kosuge, K. Soft-X-ray absorption-spectroscopy of vanadium-oxides. *Journal of Electron Spectroscopy and Related Phenomena* **1993**, *62*, 185–195.

(29) Gloter, A.; Serin, V.; Turquat, C.; Cesari, C.; Leroux, C.; Nihoul, G. Vanadium valency and hybridization in V-doped hafnia investigated by electron energy loss spectroscopy. *European Physical Journal B* **2001**, *22*, 179–186.

(30) Herrera, G.; Jimenez-Mier, J.; Wilks, R. G.; Moewes, A.; Yang, W.; Denlinger, J. Excited states in yttrium orthovanadate YVO4 measured by soft X-ray absorption spectroscopy. *Journal of Materials Science* **2013**, *48*, 6437–6444.

(31) Jimenez-Mier, J.; Olalde-Velasco, P.; Carabali-Sandoval, G.; Herrera-Perez, G.; Chavira, E.; Yang, W.-L.; Denlinger, J. X-Ray absorption to determine the metal oxidation state of transition metal compounds. Radiation physics: IX international symposium on radiation physics. 2013; pp 78–85, 9th International Symposium on Radiation Physics (ISRP), Puebla, Mexico, APR 14-17, 2013.

(32) Hopkins, E. J.; Prots, Y.; Burkhardt, U.; Watier, Y.; Hu, Z.; Kuo, C.-Y.; Chiang, J.-C.; Pi, T.-W.; Tanaka, A.; Tjeng, L. H.; Valldor, M. Ba3V2S4O3: a Mott insulating frustrated quasi-one-dimensional S=1 magnet. *Chemistry-A European Journal* **2015**, *21*, 7938–7943.

(33) Matsuura, K.; Sagayama, H.; Nii, Y.; Khanh, N. D.; Abe, N.; Arima, T. X-ray magnetic circular dichroism study of an orbital ordered state in the spinel-type vanadium oxide AV(2)O(4) (A = Mn, Fe). *Physical Review B* **2015**, *92*.

(34) Herrera-Perez, G.; Jimenez-Mier, J.; Yang, W. L.; Reyes-Rojas, A.; Fuentes-Cobas, L. E. The influence of charge transfers effects in monazite-type LaVO4 and perovskite-type LaVO3 prepared by sol-gel acrylamide polymerization. *Journal of Electron Spectroscopy and Related Phenomena* **2016**, *211*, 82–86.

(35) Kowalska, J. K.; Nayyar, B.; Rees, J. A.; Schiewer, C. E.; Lee, S. C.; Kovacs, J. A.; Meyer, F.; Weyhermueller, T.; Otero, E.; DeBeer, S. Iron L-2,L-3-edge x-ray absorption and x-ray magnetic circular dichroism studies of molecular iron complexes with relevance to the FeMoCo and FeVCo active sites of nitrogenase. *Inorganic Chemistry* **2017**, *56*, 8147–8158.

(36) Wu, M.; Zheng, J.-C.; Wang, H.-Q. Investigation of the vanadium L-23-edge x-ray absorption spectrum of SrVO3 using configuration interaction calculations: multiplet, valence, and crystal-field effects. *Physical Review B* **2018**, *95*.

(37) Schmitz, D.; Schmitz-Antoniak, C.; Radu, F.; Ryll, H.; Luo, C.; Bhandary, S.; Biermann, S.; Siemensmeyer, K.; Wende, H.; Ivanov, S.; Eriksson, O. Soft x-ray magnetic circular dichroism of vanadium in the metal-insulator two-phase region of paramagnetic V2O3 doped with 1.1% chromium. *Physica Status Solidi B-Basic Solid State Physics* **2020**, *257*.

(38) Murota, K.; Pachoud, E.; Attfield, J. P.; Glaum, R.; Sutarto, R.; Takubo, K.; Khom-

skii, D., I; Mizokawa, T. Vanadium 3d charge and orbital states in V2OPO4 probed by x-ray absorption spectroscopy. *Physical Review B* **2020**, *101*.

(39) Haverkort, M. W.; Zwierzycki, M.; Andersen, O. K. Multiplet ligand-field theory using Wannier orbitals. *Phys. Rev. B* **2012**, *85*, 165113.

(40) Wang, R.-P.; Huang, M.-J.; Hariki, A.; Okamoto, J.; Huang, H.-Y.; Singh, A.; Huang, D.-J.; Nagel, P.; Schuppler, S.; Haarman, T.; Liu, B.; de Groot, F. M. F. Analyzing the local electronic structure of Co3O4 using 2p3d resonant inelastic x-ray scattering. *Journal OF Physical Chemistry C* **2022**, *126*, 8752–8759.

(41) Huotari, S.; Sahle, C. J.; Henriquet, C.; Al-Zein, A.; Martel, K.; Simonelli, L.; Verbeni, R.; Gonzalez, H.; Lagier, M.-C.; Ponchut, C., et al. A large-solid-angle X-ray Raman scattering spectrometer at ID20 of the European Synchrotron Radiation Facility. *Journal of synchrotron radiation* **2017**, *24*, 521–530.

(42) Sahle, C. J.; Mirone, A.; Niskanen, J.; Inkinen, J.; Krisch, M.; Huotari, S. Planning, performing and analyzing X-ray Raman scattering experiments. *Journal of synchrotron radiation* **2015**, *22*, 400–409.

(43) Kresse, G.; Joubert, D. From ultrasoft pseudopotentials to the projector augmented-wave method. *Physical Review B* **1999**, *59*, 1758–1775.

(44) Blöchl, P. E. Projector augmented-wave method. *Physical Review B* **1994**, *50*, 17953–17979.

(45) Kresse, G.; Hafner, J. *Ab initio* molecular dynamics for liquid metals. *Physical Review B* **1993**, *47*, 558–561.

(46) Kresse, G.; Furthmüller, J. Efficiency of ab-initio total energy calculations for metals and semiconductors using a plane-wave basis set. *Computational Materials Science* **1996**, *6*, 15–50.

(47) Kresse, G.; Furthmüller, J. Efficient iterative schemes for *ab initio* total-energy calculations using a plane-wave basis set. *Physical Review B* **1996**, *54*, 11169–11186.

(48) Kresse, G.; Hafner, J. *Ab initio* molecular-dynamics simulation of the liquid-metal–amorphous-semiconductor transition in germanium. *Physical Review B* **1994**, *49*, 14251–14269.

(49) Perdew, J. P.; Burke, K.; Ernzerhof, M. Generalized gradient approximation made simple. *Physical Review Letters* **1996**, *77*, 3865–3868.

(50) Dudarev, S. L.; Botton, G. A.; Savrasov, S. Y.; Humphreys, C. J.; Sutton, A. P. Electron-energy-loss spectra and the structural stability of nickel oxide: An LSDA+U study. *Physical Review B* **1998**, *57*, 1505–1509.

(51) Kim, H.; Seo, D.-H.; Bianchini, M.; Clément, R. J.; Kim, H.; Kim, J. C.; Tian, Y.; Shi, T.; Yoon, W.-S.; Ceder, G. A new strategy for high-voltage cathodes for K-ion batteries: stoichiometric KVPO $_4$ F. *Advanced Energy Materials* **2018**, *8*, 1801591.

(52) Carlier, D.; Ménétrier, M.; Grey, C. P.; Delmas, C.; Ceder, G. Understanding the NMR shifts in paramagnetic transition metal oxides using density functional theory calculations. *Physical Review B* **2003**, *67*, 174103.

(53) Mirone, A.; Sacchi, M.; Gota, S. Ligand-field atomic-multiplet calculations for arbitrary symmetry. *Phys. Rev. B* **2000**, *61*, 13540–13544.

(54) de Groot, F. M. et al. 2p x-ray absorption spectroscopy of 3d transition metal systems. *Journal of Electron Spectroscopy and Related Phenomena* **2021**, *249*, 147061.

(55) de Groot, F. Multiplet effects in X-ray spectroscopy. *Coordination Chemistry Reviews* **2005**, *249*, 31–63, Synchrotron Radiation in Inorganic and Bioinorganic Chemistry.

(56) Giannozzi, P.; Baroni, S.; Bonini, N.; Calandra, M.; Car, R.; Cavazzoni, C.; Ceresoli, D.; Chiarotti, G. L.; et al., M. C. Quantum Espresso: a modular and open-source software

project for quantum simulations of materials. *Journal of Physics: Condensed Matter* **2009**, *21*, 395502.

(57) Giannozzi, P.; Andreussi, O.; Brumme, T.; Bunau, O.; Nardelli, M. B.; Calandra, M.; Car, R.; Cavazzoni, C.; Ceresoli, D.; al., M. C. Advanced capabilities for materials modelling with Quantum Espresso. *Journal of Physics: Condensed Matter* **2017**, *29*, 465901.

(58) Mostofi, A. A.; Yates, J. R.; Lee, Y.-S.; Souza, I.; Vanderbilt, D.; Marzari, N. wannier90: A tool for obtaining maximally-localised Wannier functions. *Computer Physics Communications* **2008**, *178*, 685–699.

(59) Mostofi, A. A.; Yates, J. R.; Pizzi, G.; Lee, Y.-S.; Souza, I.; Vanderbilt, D.; Marzari, N. An updated version of wannier90: A tool for obtaining maximally-localised Wannier functions. *Computer Physics Communications* **2014**, *185*, 2309–2310.

(60) Edmonds, A. R. *Angular momentum in quantum mechanics*; Princeton University Press: Princeton, 2016.

(61) Joly, Y.; Cavallari, C.; Guda, S. A.; Sahle, C. J. Full-potential simulation of x-ray Raman scattering spectroscopy. *Journal of Chemical Theory and Computation* **2017**, *13*, 2172–2177.

(62) Benhamada, L.; Grandin, A.; Borel, M. M.; Leclaire, A.; Raveau, B. $KVPO_5$, an intersecting tunnel structure closely related to the hexagonal tungsten bronze. *Acta Crystallographica Section C Crystal Structure Communications* **1991**, *47*, 1138–1141.

(63) Fedotov, S. S.; Khasanova, N. R.; Samarin, A. S.; Drozhzhin, O. A.; Batuk, D.; Karakulina, O. M.; Hadermann, J.; Abakumov, A. M.; Antipov, E. V. $AVPO_4F$ (A = Li, K): A 4 V cathode material for high-power rechargeable batteries. *Chemistry of Materials* **2016**, *28*, 411–415.

(64) Thole, B. T.; van der Laan, G. Branching ratio in x-ray absorption spectroscopy. *Phys. Rev. B* **1988**, *38*, 3158–3171.

TOC Graphic

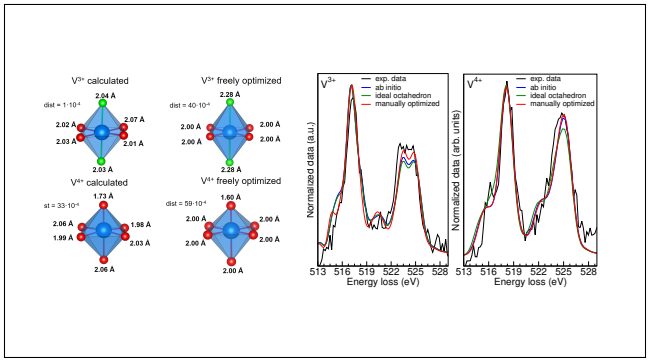
V3+ calculated
dist = 1·10-4
2.04 Å
2.07 Å
2.02 Å
2.03 Å
2.01 Å
2.03 Å
V3+ freely optimized
dist = 40·10-4
2.28 Å
2.00 Å
2.00 Å
2.00 Å
2.00 Å
2.28 Å
V4+ calculated
st = 33·10-4
1.73 Å
2.06 Å
1.98 Å
1.99 Å
2.03 Å
2.06 Å
V4+ freely optimized
dist = 59·10-4
1.60 Å
2.00 Å
2.00 Å
2.00 Å
2.00 Å
2.00 Å
V3+
exp. data
ab initio
ideal octahedron
manually optimized
Normalized data (a.u.)
513 516 519 522 525 528
Energy loss (eV)
V4+
exp. data
ab initio
ideal octahedron
manually optimized
Normalized data (arb. units)
513 516 519 522 525 528
Energy loss (eV)